Available online at www.sciencedirect.com
ScienceDirect
Polymer 47 (2006) 7760–7773
polymer
www.elsevier.com/locate/polymer

Morphology and properties of thermoplastic polyurethane nanocomposites: Effect of organoclay structure

F. Chavarria, D.R. Paul*

Department of Chemical Engineering and Texas Materials Institute, The University of Texas at Austin, Austin, TX 78712-1062, USA

Received 27 June 2006; received in revised form 23 August 2006; accepted 27 August 2006
Available online 25 September 2006

Abstract

A series of alkyl ammonium/MMT organoclays were carefully selected to explore structure–property relationships for thermoplastic polyurethane (TPU) nanocomposites prepared by melt processing. Each organoclay was melt-blended with a medium-hardness, ester-based TPU, while a more limited number of organoclays was blended with a high-hardness, ether-based TPU. Wide-angle X-ray scattering, transmission electron microscopy, particle analysis, and stress–strain behavior were used to examine the effects of organoclay structure and TPU chemical structure on morphology and mechanical properties. Specifically, the following were observed: (a) one long alkyl tail on the ammonium ion rather than two, (b) hydroxy ethyl groups on the amine rather than methyl groups, and (c) a longer alkyl tail as opposed to a shorter one leads to higher clay dispersion and stiffness for medium-hardness TPU nanocomposites. Overall, the organoclay containing hydroxy ethyl functional groups produces the best dispersion of organoclay particles and the highest matrix reinforcement, while the one containing two alkyl tails produces the poorest. The two TPU's exhibit similar trends with regard to the effect of organoclay structure. The high-hardness TPU nanocomposites showed a slightly higher number of particles and clay dispersion. The organoclay structure trends are analogous to what has been observed for nylon 6-based nanocomposites; this suggests that polar polymers like polyamides, and apparently polyurethanes, have a relatively good affinity for the polar clay surface; and in the case of polyurethanes, the high affinity of the matrix for the hydroxy ethyl functional groups in the organoclay aids clay dispersion and exfoliation.

Keywords: Thermoplastic polyurethane; Nanocomposites; Melt processing

1. Introduction

Research on polymer layered silicate nanocomposites has been intense over the last few years as a result of the potentially superior properties that these materials can exhibit compared to conventional composites. Numerous studies have shown that the addition of a very low percentage of layered silicates can lead to a significant enhancement in many properties, such as stiffness and strength [1–3], flame retardancy [4,5], gas barrier properties [6], ionic conductivity [7,8], thermal stability [9], and tunable biodegradability [4]. All these properties make these materials interesting prospects for a wide variety of applications, e.g., automotive, electronics, food packaging, biotechnology, and others.

Polymer layered silicate nanocomposites are typically made from organoclays composed of sodium montmorillonite (MMT) cationically exchanged with alkyl ammonium surfactants that expand the interlayer distance of the clay and make it more organophilic. The key to obtain significant property enhancements is to disperse, or exfoliate, the individual silicate platelets within the polymer matrix to take advantage of their high aspect ratio and surface area. The affinity of the polymer with the surface of the clay and/or with the organic surfactant of the organoclay is essential to promote favorable interactions between these species and, hence, to obtain high levels of exfoliation.

The affinity between the polymer matrix and the organoclay is determined, to some extent, by the polarity of the

* Corresponding author. Tel.: +1 512 471 5392; fax: +1 512 471 0542.
E-mail address: drp@che.utexas.edu (D.R. Paul).

0032-3861/$ - see front matter © 2006 Elsevier Ltd. All rights reserved.
doi:10.1016/j.polymer.2006.08.067

polymer and the type of organic modifier used to form the organoclay. Recent studies from our laboratory have shown that a polar polymer such as nylon 6 (PA-6), exhibits a higher level of exfoliation with an organoclay based on a surfactant with one alkyl tail, while nanocomposites made from non-polar polymers, such as polypropylene, polyethylene, and various copolymers show completely opposite trends, i.e., organoclays based on surfactants with two or more alkyl tails lead to more exfoliated nanocomposites than a one-tailed organoclay [10–13]. Since a one-tailed organoclay provides less coverage of the silicate surface than a two-tailed organoclay, these results suggest that PA-6 has a higher affinity for the polar surface of the clay than for the largely non-polar surfactant, while the opposite is true for non-polar matrices.

Thermoplastic polyurethanes (TPU's) have similar functional groups as PA-6 but rather different repeat unit structures. There is a growing literature on polyurethane nanocomposites describing, among other things, the effect of methods of preparation, polyurethane and organoclay structure, and hard segment concentration on degree of clay dispersion or exfoliation, microphase morphology, hydrogen bonding, rheology, mechanical properties, thermal stability, flame retardancy, water sorption, and barrier properties [2,14–27]. There are very few reports on polyurethane nanocomposites prepared by melt processing [20,21] in spite of the obvious advantages of this approach [28–30].

The objective of this study is to explore the effect of the surfactant chemical structure on the morphology and mechanical properties of TPU nanocomposites prepared by melt processing. Detailed comparisons of the structure of the organic treatment (such as number of alkyl tails, saturation of the alkyl chain, different side groups, and length of the alkyl chain) are reported here for nanocomposites formed from a medium-hardness TPU. A more limited study of nanocomposites based on high-hardness TPU is also reported. Mechanical properties and morphology characterization are used to evaluate the structure and performance of these composites.

2. Experimental

2.1. Materials

The materials used in this study are described in Table 1. Two commercial grades of thermoplastic polyurethane were selected for this work; one was a medium-hardness polyester-based TPU from Dow Plastics and the other was a high-hardness polyether-based TPU from BASF. The medium- and high-hardness thermoplastic polyurethanes will be referred to as M-H and H-H TPU's, respectively. Several amine based organoclays from Southern Clay Products were chosen to determine the effect of the number of long alkyl tails, $M_3(HT)_1$ vs. $M_2(HT)_2$, saturation of the primary tail, M_3T_1 vs. $M_3(HT)_1$, the effect of hydroxy ethyl functional groups, $(HE)_2M_1T_1$ vs. M_3T_1, and length of the alkyl tail, $(HE)_2M_1T_1$ vs. $(HE)_2M_1C_1^*$. The chemical structures of the alkyl ammonium surfactants used to form the organoclays are shown in Fig. 1. All data are reported in terms of weight percent montmorillonite, wt% MMT, in the composite rather than the amount of organoclay, since the silicate is the reinforcing component. The amount of MMT was determined by heating extruded pellets in a furnace at 900 °C for 45 min and weighing the remaining MMT ash correcting for loss of structural water during incineration [29].

Table 1
Materials used in this study

Material (designation used in this paper)	Supplier designation	Specifications[b]	Supplier
Thermoplastic polyurethanes			
Medium-hardness TPU (M-H TPU)	Pellethane 9102-90AE	Polyester-based TPU *Methylenediphenyl diisocyanate* *1,4-Butanediol* *ε-Caprolactone* Shore D hardness = 58 D	Dow Plastics
High-hardness TPU (H-H TPU)	Elastollan 1174D50	Polyether-based TPU *Methylenediphenyl diisocyanate* *Poly(tetrahydrofuran)* Shore D hardness = 73 D	BASF
Organoclays[a]			
$M_3(HT)_1$	*Experimental*: trimethyl hydrogenated-tallow ammonium chloride organoclay	95 MER, organic content = 29.6 wt%, d_{001} spacing = 18.0 Å	Southern Clay Products
$M_2(HT)_2$	*Cloisite® 20A*: dimethyl bis(hydrogenated-tallow) ammonium chloride organoclay	95 MER, organic content = 39.6 wt%, d_{001} spacing = 24.2 Å	Southern Clay Products
M_3T_1	*Experimental*: trimethyl tallow quaternary ammonium chloride organoclay	95 MER, organic content = 29.1 wt%, d_{001} spacing = 17.8 Å	Southern Clay Products
$(HE)_2M_1T_1$	*Cloisite® 30B*: bis(2-hydroxy-ethyl)methyl tallow ammonium chloride organoclay	90 MER, organic content = 31.5 wt%, d_{001} spacing = 17.9 Å	Southern Clay Products
$(HE)_2M_1C_1^*$	*Experimental*: bis(2-hydroxy-ethyl)methyl coco ammonium chloride organoclay	95 MER, organic content = 26.4 wt%, d_{001} spacing = 15.2 Å	Southern Clay Products

[a] Short hand notations for substituents on ammonium compounds: M = methyl, HT = hydrogenated-tallow, T = tallow, HE = hydroxy-ethyl, and C* = coco. Tallow and coco are natural products composed predominantly of unsaturated C_{18} alkyl chains (65%) and C_{12} alkyl chains (48%), respectively.
[b] MER = The organic content in terms of milliequivalents of amine salt/100 g of clay.

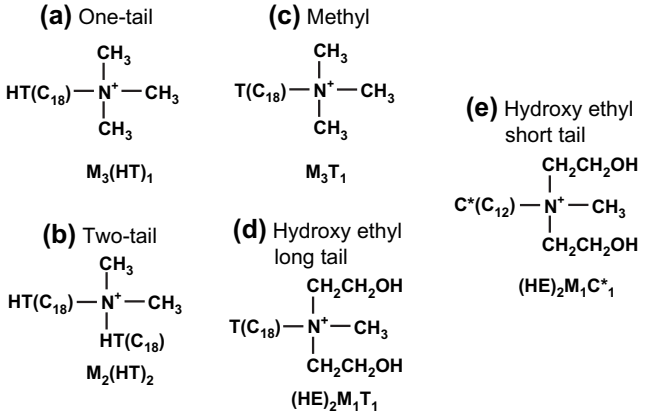

Fig. 1. Molecular structure and nomenclature of the amines used to form the organoclays used in this study.

2.2. Melt processing

TPU nanocomposites were prepared by melt compounding in a Haake, co-rotating, intermeshing twin screw extruder ($D = 30$ mm, $L/D = 10$) at a screw speed of 280 rpm, a feed rate of 1200 g/h, and a temperature of 190 °C. Prior to each processing step, all materials containing thermoplastic polyurethane were dried in a vacuum oven at 80 °C for a minimum of 16 h.

Dried extruded pellets were injection molded into standard tensile bars (ASTM D638) using an Arburg Allrounder 305-210-700 injection molding machine. A barrel temperature range of 200–215 °C from feed to nozzle was used for the M-H TPU materials, while a range of 180–200 °C was used for the H-H TPU materials. A mold temperature of 50 °C, injection pressure of 70 bar, and holding pressure of 65 bar were used for both materials. After molding, the specimens were sealed and placed in a vacuum desiccator for a minimum of 24 h prior to mechanical testing.

2.3. Characterization

Tensile tests were conducted according to ASTM D638 using an Instron 1137 testing machine. Modulus was determined using an extensometer at a crosshead speed of 0.51 cm/min. Elongation at break was obtained from crosshead travel using an effective gauge length of 9.04 cm and a crosshead speed of 5.1 cm/min. Tensile stress at 300% elongation was reported, due to its standard use in the polyurethane literature; it will be referred to as the 300% stress. The values reported here represent an average of five specimens for modulus, and three to four specimens for elongation at break and 300% stress; standard deviations were typically of the order of 3% for modulus, and 1–30% for elongation at break. The values reported for 300% stress were obtained from the most representative stress–strain curve.

Wide-angle X-ray diffraction (WAXD) scans were made using a Scintag XDS 2000 diffractometer in reflection mode, with an incident wavelength of 0.154 nm at a scan rate of 1.0°/min. The analysis was performed using tensile bars for the polymer samples while the clay was analyzed in powder form.

Transmission electron microscopic (TEM) images were obtained using a JEOL 2010F transmission electron microscope operating at an accelerating voltage of 120 kV and a Phillips EM208 transmission electron microscope with an accelerating voltage of 80 kV. Samples for TEM were cryogenically cut into ultra thin sections (50–70 nm thick) with a diamond knife at a temperature of −40 °C using an RMC PowerTome XL ultramicrotome with a CR-X universal cryosectioning system. These sections were taken from the central part of a tensile bar normal to the flow direction and viewed in the TEM parallel to the flow direction (FD). Scanning transmission electron microscopy (STEM) images were obtained using a JEOL 2010F transmission electron microscope operating in the dark-field, scanning mode at an accelerating voltage of 200 kV.

The TEM images shown in this manuscript are representative of the morphologies of the nanocomposites observed through TEM; hence, the particle analysis results from the procedure described below may not be in exact accord with the observations from a single image since they represent averages over a much larger sample area. The analyses were done to ensure an objective and accurate representation of the morphology of the nanocomposite systems.

2.4. Particle analysis

Particle analysis was done with Adobe Photoshop, using three TEM micrographs, at 25K magnification, for each sample. The average particle length was determined by tracing the clay particles electronically, within Adobe Photoshop, into a transparent layer [31] similar to the procedure used in a previous study [32]. The area of interest was also traced into a transparent layer within Adobe Photoshop. The measurements of particle length and area were determined using IPTK™ 5.0, a commercially available set of plug-ins, for use with Adobe Photoshop, developed by Reindeer Graphics Inc. [33]. The average particle density was considered as the average number of particles per μm^2. The specific particle density is the average particle density normalized to a specific clay concentration (in this study, the specific clay concentrations will be 1 and 5.5 wt% MMT). These values are a measure of the extent of exfoliation of the organoclay in the polymer matrix.

3. Results and discussion

3.1. Effect of organic modifier for the M-H TPU

The following results show the effect of organoclay structure on morphology and properties of nanocomposites prepared from the medium-hardness TPU. Morphology, as judged by WAXD, TEM, particle analysis, and dark-field STEM, and mechanical properties, assessed by Young's modulus, 300% stress, and elongation at break, are used to characterize the structure–property relationship of these materials.

3.1.1. Clay dispersion

Fig. 2 shows WAXD scans for various nanocomposites made in this study containing ~2.3 wt% MMT, along with a scan of

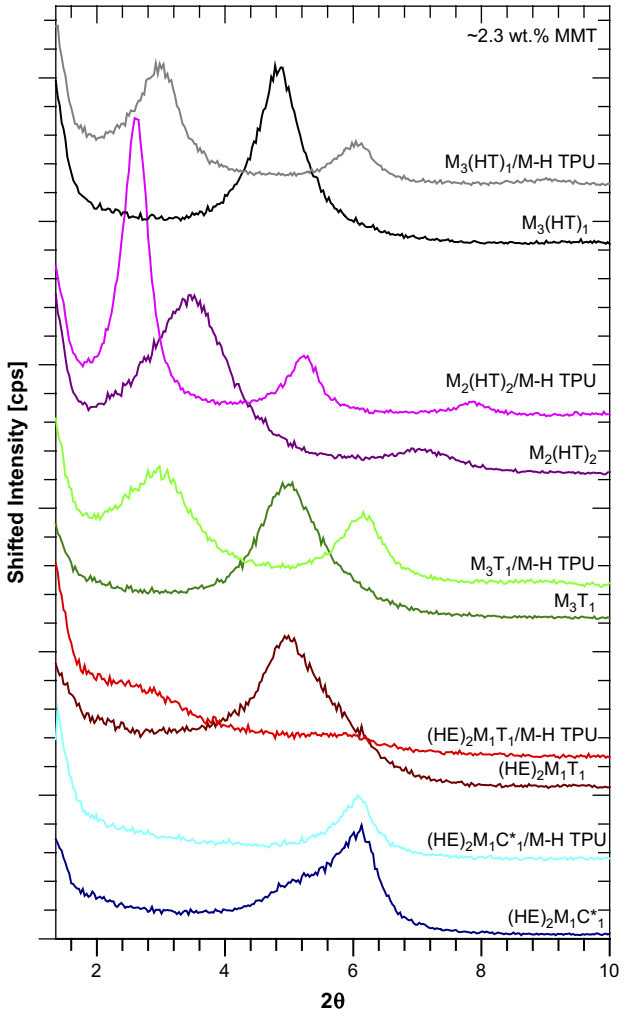

Fig. 2. WAXD patterns for pure organoclays and their respective M-H TPU nanocomposites containing ~2.3 wt% MMT.

each organoclay for comparison. In every case, the nanocomposite scans show basal reflections indicating that all the nanocomposites contain tactoids of organoclay with high enough order and concentration to diffract X-rays. There is an increase in the *d*-spacing of all the nanocomposites with respect to that of the pure organoclays, except for the samples containing the $(HE)_2M_1C_1^*$ surfactant. The increase in *d*-spacing for the nanocomposites made with $M_3(HT)_1$ is from 1.8 to 2.9 nm, while those for $M_2(HT)_2$ shows a slightly smaller increase from 2.55 to 3.41 nm. M_3T_1 shows an increase in *d*-spacing from 1.75 to 2.96 nm and $(HE)_2M_1T_1$ shows a weaker and more diffuse peak that seems to be centered around 3.05 nm, with respect to 1.77 nm of the organoclay. According to conventional interpretations, this suggests some degree of polymer intercalation into the organoclay galleries. It should be noted that the WAXD patterns in Fig. 2 show only one basal reflection for the organoclays, while more high-order reflections were observed for the nanocomposite samples. The organoclay scans were made from powders while the nanocomposite scans were made from the surface of injection molded samples. The greater orientations in the latter lead to multiple reflections while the more random orientations of the organoclay powders do not.

TEM micrographs shown in Figs. 3 and 4 provide additional insight about the morphology of these nanocomposites. At low concentrations, all the composites have a similar structure, except for the sample containing $(HE)_2M_1T_1$, which shows a noticeably higher number of particles. At high concentrations, the nanocomposites from $(HE)_2M_1T_1$ also have the highest number of particles with the smallest size. The nanocomposites containing $M_3(HT)_1$ and M_3T_1 have a somewhat lower number of particles of slightly larger size; while the samples containing $(HE)_2M_1C_1^*$ show a mixture of small particles and larger agglomerates. The two-tailed organic modifier ($M_2(HT)_2$) produces the lowest number of particles with the largest size. At the same clay concentration, the particle count is an indicator of the extent of exfoliation of clay platelets in the polymer matrix. Samples with a low particle count have large particles with high platelet agglomeration and, as the particle count increases, the particle size decreases as a result of the breakup of large particles, producing better dispersion.

The number of long alkyl tails on the surfactant in the organoclay affects the morphology of these TPU nanocomposites (Fig. 3a and b). $M_2(HT)_2$ leads to a small number of large, extended tactoids, while $M_3(HT)_1$ produces a higher number of small, elongated tactoids. The unsaturated surfactant, M_3T_1, produces a very similar morphology as that obtained from the saturated organoclay, $M_3(HT)_1$, but there seems to be a larger number of particles and more alignment in the nanocomposites made from the saturated organoclay (Fig. 3b and c). The surfactant with hydroxy ethyl functional groups, $(HE)_2M_1T_1$, leads to the smallest tactoids and many particles are single platelets. There is a higher particle count, or a higher degree of clay dispersion in the samples containing hydroxy ethyl groups than in the ones containing methyl substituents (Fig. 4a and b). The length of the alkyl tail also seems to affect clay dispersion, as seen in Fig. 4b and c; the shorter alkyl tail does not produce as high clay dispersion as the longer alkyl.

These qualitative trends in Figs. 3 and 4 are quantified by particle analysis of TEM images; the results are shown in Table 2. The complex shapes of the clay particles in TPU nanocomposites made thickness estimation very difficult, so values of aspect ratios for these samples could not be obtained. Nevertheless, measurements of particle lengths and densities give insight about the degree of platelet dispersion of these nanocomposites. At low concentrations, the particle lengths are very similar for all the samples, while the specific particle density is highest in the samples made with $(HE)_2M_1T_1$, as seen in the TEM micrographs. At high concentrations, the samples made from $M_2(HT)_2$ have the highest particle length, while the ones made from $(HE)_2M_1T_1$ have the lowest. The specific particle density is again highest for the nanocomposites made from the $(HE)_2M_1T_1$ organoclay, suggesting the highest degree of dispersion, while $M_2(HT)_2$ produces an extremely low particle density consistent with the large agglomerates seen in TEM. High matrix reinforcement might be expected from a high particle density; however, the aspect ratio of the filler particles is the true parameter needed to assess the degree of reinforcement.

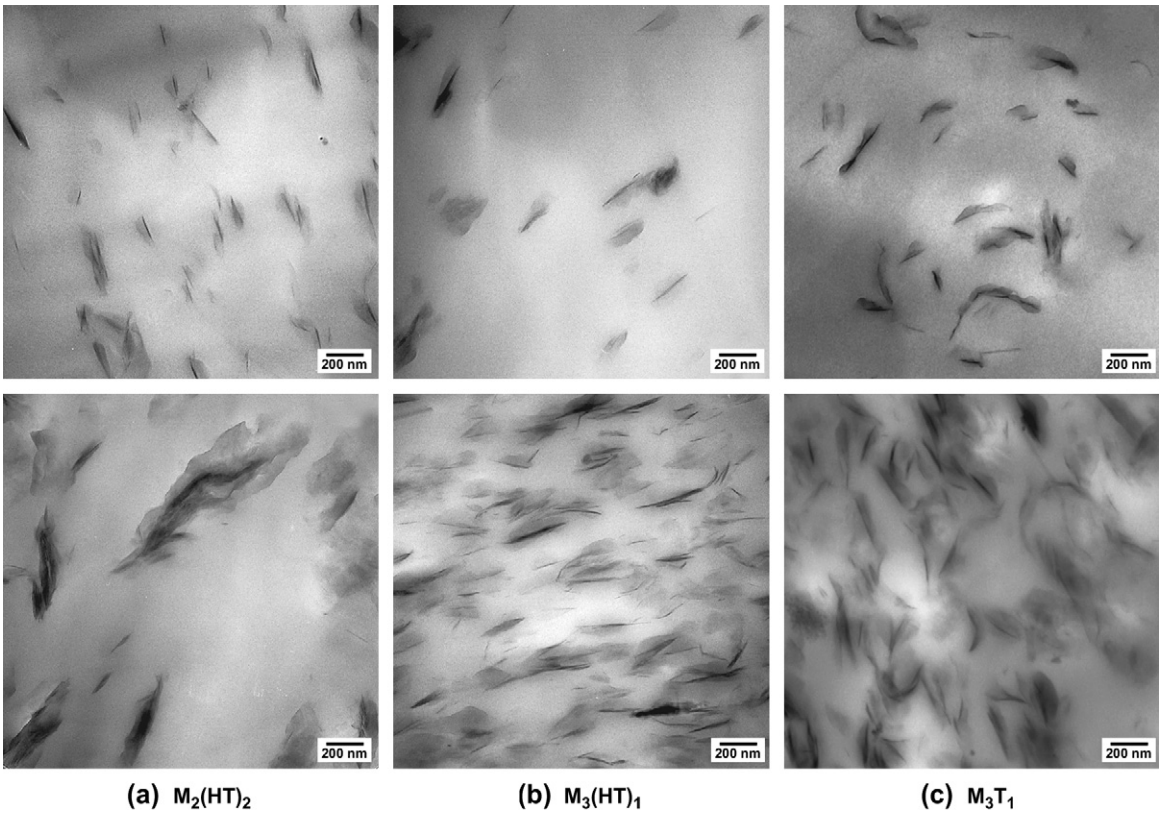

Fig. 3. TEM micrographs for nanocomposites based on M-H TPU and organoclays: (a) $M_2(HT)_2$, (b) $M_3(HT)_1$, and (c) M_3T_1; with concentrations ranging from 0.48 to 0.94 wt% MMT (above) and from 4.61 to 6 wt% MMT (below).

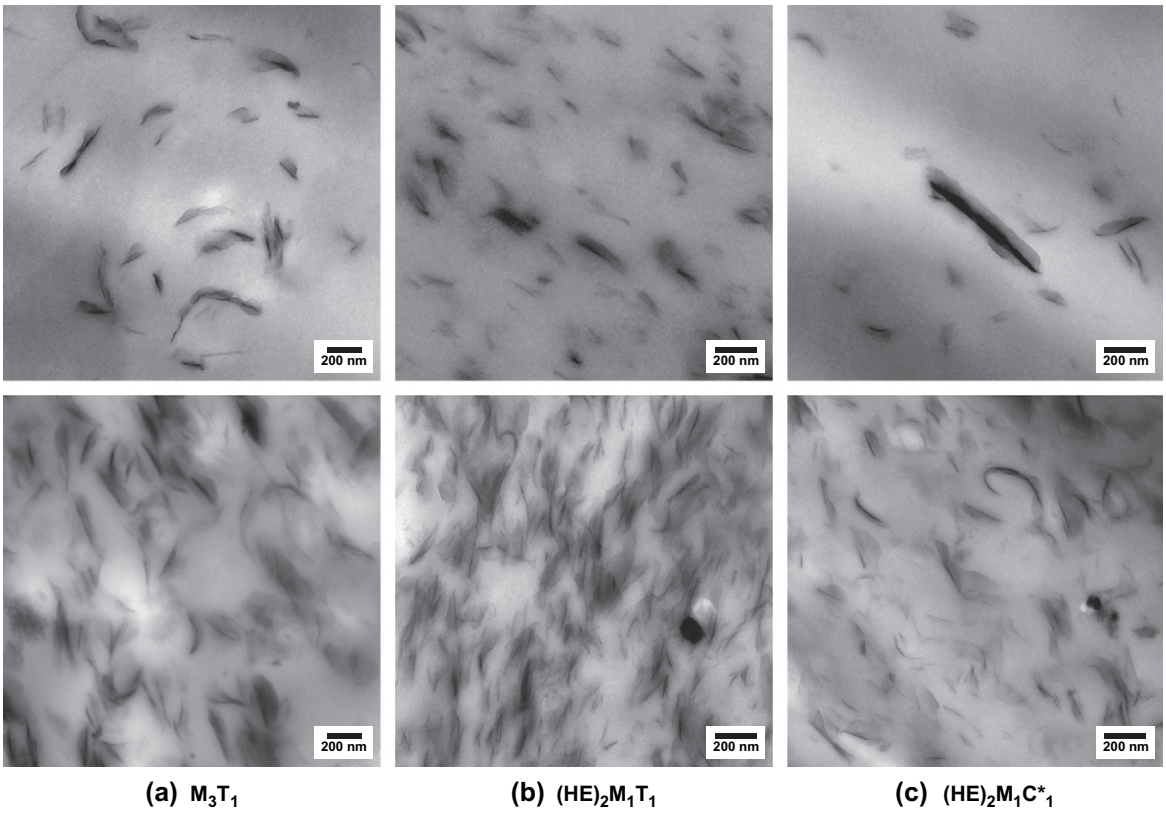

Fig. 4. TEM micrographs for nanocomposites based on M-H TPU and organoclays: (a) M_3T_1, (b) $(HE)_2M_1T_1$, and (c) $(HE)_2M_1C_1^*$; with concentrations ranging from 0.9 to 0.95 wt% MMT (above) and from 5.46 to 6 wt% MMT (below).

Table 2
Particle analysis results of M-H TPU nanocomposites

Organoclay nanocomposites	No. of particles analyzed	Particle length (nm)		Particle density (particles/μm^2)	Specific particle density (particles/μm^2)
		Number average	Weight average		
$M_3(HT)_1$					
0.48 wt% MMT	159	138 ± 3	172 ± 11	8 ± 2	16 ± 4
5.05 wt% MMT	842	141 ± 7	183 ± 12	43 ± 4	47 ± 5
$M_2(HT)_2$					
0.61 wt% MMT	233	113 ± 7	144 ± 7	11 ± 3	19 ± 4
4.61 wt% MMT	182	215 ± 31	327 ± 31	10 ± 1	12 ± 1
M_3T_1					
0.94 wt% MMT	541	142 ± 6	180 ± 12	9 ± 1	10 ± 1
6.00 wt% MMT	1311	191 ± 7	248 ± 16	22 ± 1	21 ± 1
$(HE)_2M_1T_1$					
0.9 wt% MMT	946	114 ± 10	142 ± 10	28 ± 4	31 ± 5
5.46 wt% MMT	1376	118 ± 2	149 ± 2	93 ± 12	93 ± 12
$(HE)_2M_1C^*_1$					
0.95 wt% MMT	546	135 ± 7	184 ± 19	10 ± 1	10 ± 1
5.68 wt% MMT	897	133 ± 12	132 ± 17	56 ± 7	54 ± 7

The complex shapes of the clay particles in TPU nanocomposites were explored by comparing bright-field TEM and dark-field STEM images. When using the dark-field STEM technique, the MMT platelets appear white, while the polymer matrix, holes in the specimen, or any other low-atomic-density constituent are seen as a black background. Fig. 5 confirms

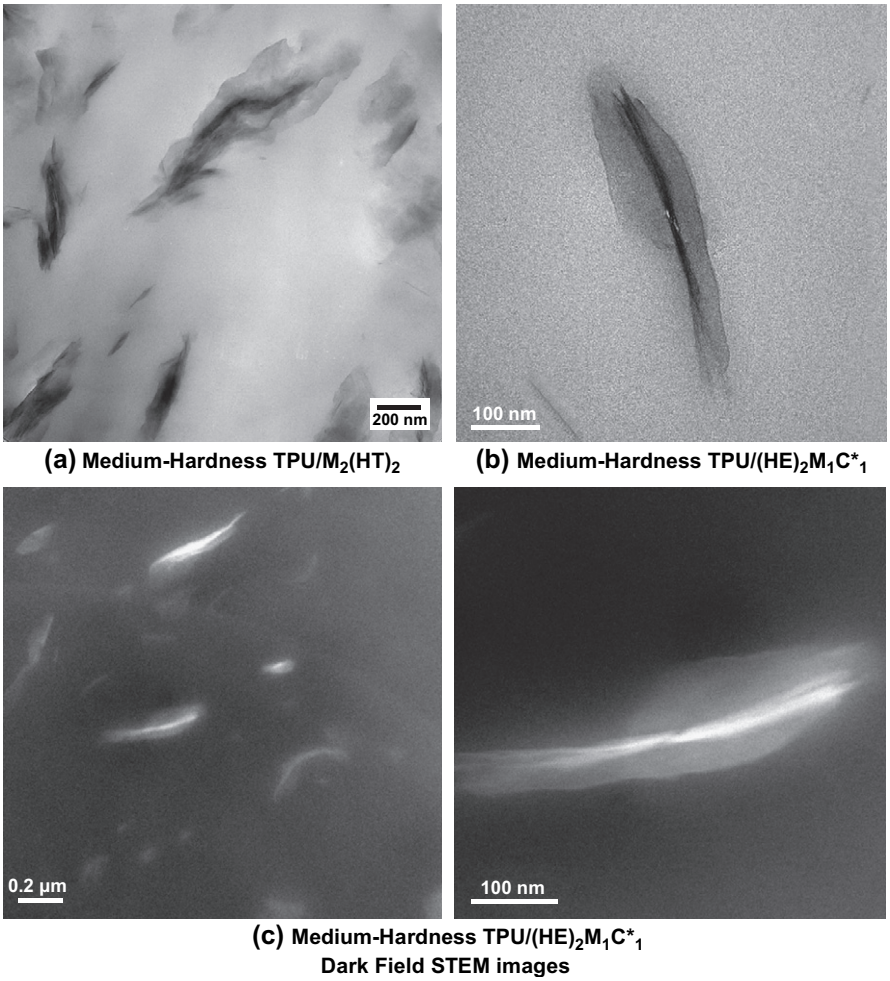

Fig. 5. Dark-field analysis of M-H TPU nanocomposite particles. Above: bright-field TEM images of M-H TPU nanocomposites (low magnification many particles (left) and high magnification showing one particle (right)). Below: dark-field STEM images of M-H TPU nanocomposites (low magnification showing many particles (left) and high magnification showing one particle (right)).

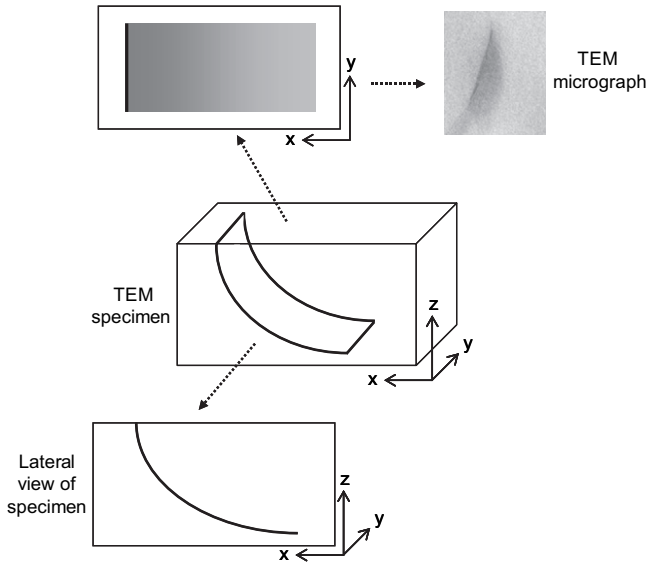

Fig. 6. Schematic illustration of possible platelet orientation for a TEM image of a clay particle with a grey area on one side of a particle.

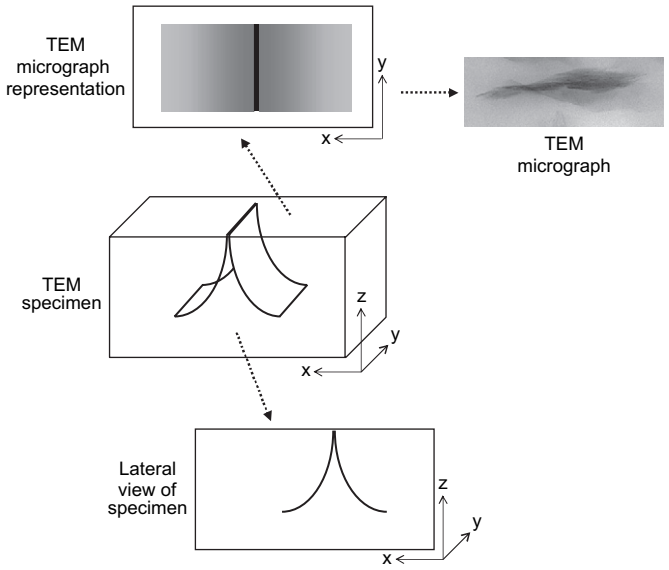

Fig. 7. Schematic illustration of possible platelet orientation for a TEM image of a clay particle with grey areas on both sides of the particle: particle with one or many platelets separated on the far side of the sample.

that the small grey areas seen around some of the particles in the bright-field TEM images are in fact clay. In a specific example, Fig. 5c shows that the grey area surrounding the particle in Fig. 5b is white, which suggests the presence of one or more MMT platelets. In bright-field TEM, sharp lines show platelet edges, i.e., the platelets are aligned with the electron beam, while grey areas of different intensities show one or more skewed or misaligned platelets. A careful analysis of the TEM images has led us to suggest a series of possible platelet orientations within the microtomed section that might explain the clay morphologies seen by TEM. Images containing particles with a grey area on only one side of a sharp line may be the result of a platelet oriented within the microtomed section as suggested in Fig. 6; the sharp line being the edge of the platelet aligned with the electron beam, and the grey area being the skewed body. Particles with grey areas on both sides of sharp edges suggest more complex configurations of what is described in Fig. 6. Figs. 7 and 8 illustrate how grey areas on both sides might involve having a particle with one or many platelets separated on the far side of the section, or a particle with many platelets skewed towards one side. As shown before, TEM images of some TPU nanocomposites have particles containing sharp dark areas in the center, surrounded by large grey areas. It is proposed that these images represent particles with aligned platelets in the center, surrounded by a smaller number of disordered platelets with no edges on the electron beam path. TEM micrographs taken with the view parallel to the normal direction (ND) (i.e., in the flow direction–transverse direction (FD–TD) plane) show the same morphology, indicating that this condition might be present in all directions (Fig. 9).

3.1.2. Mechanical properties

Fig. 10 shows representative stress–strain curves for the nanocomposites prepared in this study and illustrate three distinctive types of behaviors. Addition of clay produces an increase in the modulus at small strains in all cases; however, the different organoclays affect the large strain behavior in different ways and may even produce limitations on elongation. In the stress–strain curve for the nanocomposites made from $(HE)_2M_1T_1$, the stress is increased at all strains as the concentration of clay increases (Fig. 10a). This was also observed for the stress–strain curves of the nanocomposites made with $(HE)_2M_1C_1^*$, and M_3T_1, but to a lesser extent. The opposite behavior is observed in the stress–strain diagram for the nanocomposites made with $M_2(HT)_2$ (Fig. 10c), as the clay concentration is increased, the stress levels at high strains are

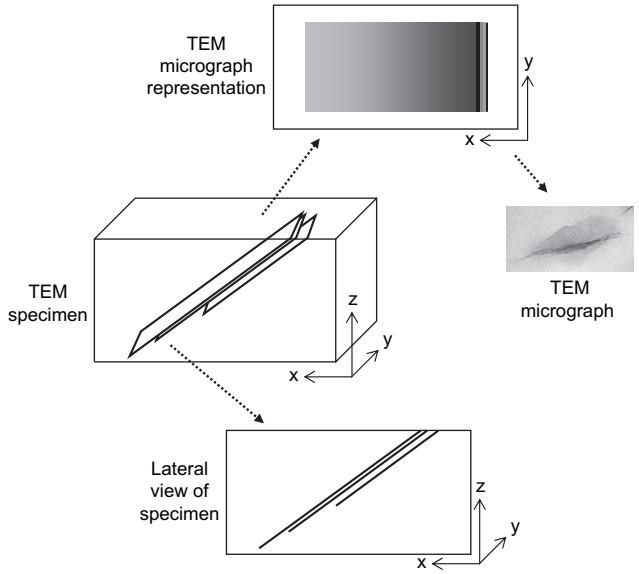

Fig. 8. Schematic illustration of possible platelet orientation for a TEM image of a clay particle with grey areas on both sides of the particle: particle with many platelets, all skewed towards one side.

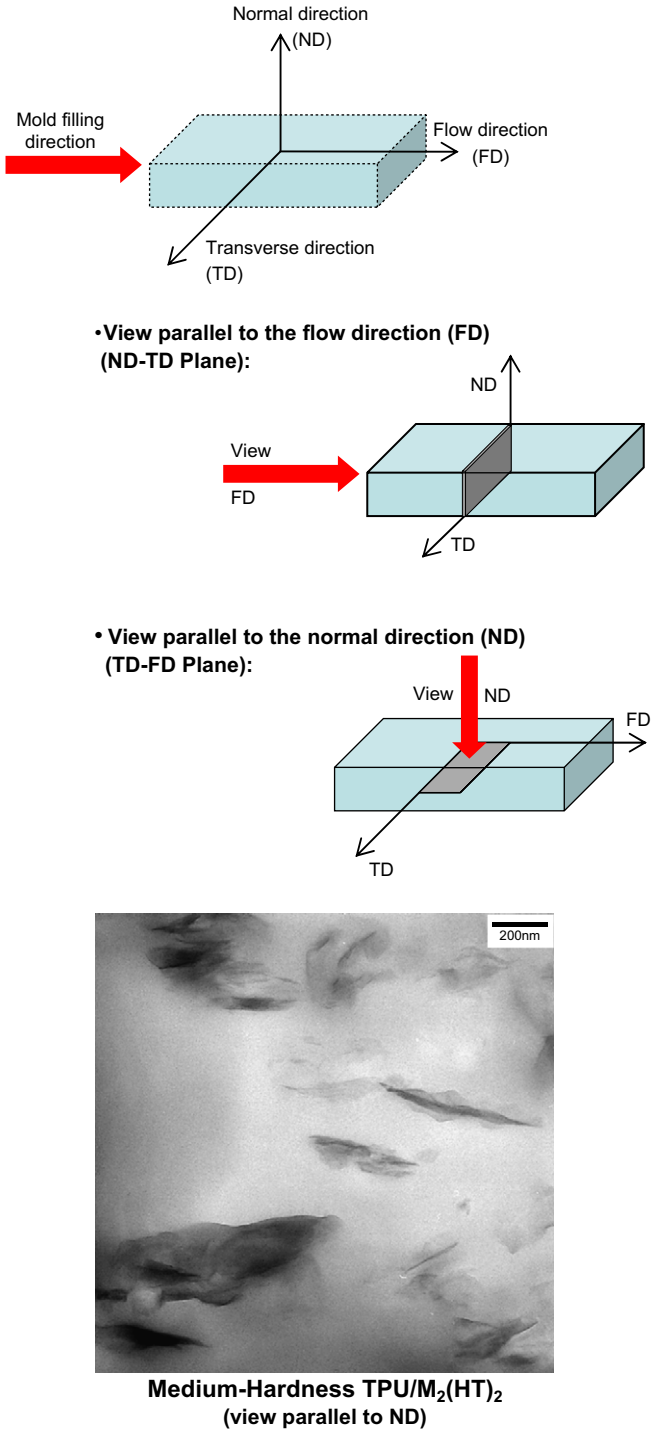

Fig. 9. TEM sample orientations used in this work and TEM image of TPU/$M_2(HT)_2$ nanocomposites (viewed parallel to the normal direction).

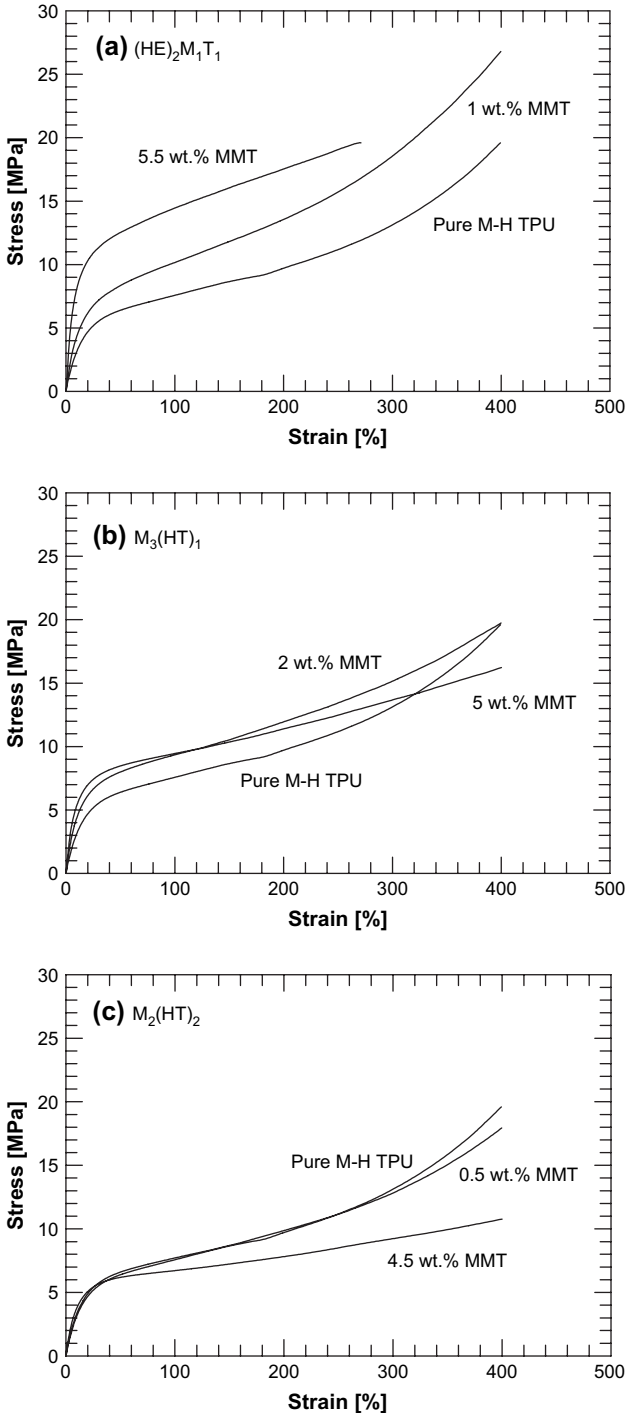

Fig. 10. Stress–strain behavior of M-H TPU and its nanocomposites: (a) $(HE)_2M_1T_1$, (b) $M_3(HT)_1$, and (c) $M_2(HT)_2$.

reduced. An intermediate behavior is seen for the nanocomposites made with $M_3(HT)_1$, where the stress at low clay concentrations is higher than that of the pristine TPU, but lower at high clay concentrations (Fig. 10b). This suggests that at high strains, the $(HE)_2M_1T_1$ organoclay continues to reinforce the TPU even at high clay concentrations, $M_3(HT)_1$ provides high strain reinforcement only at low clay concentrations, while $M_2(HT)_2$ does not reinforce the polyurethane matrix at high strains. The elongated tensile bars show signs of permanent set and stress whitening; both increase as the clay concentration increases. The permanent set is highest for the samples made from $M_2(HT)_2$, followed by the ones made with $M_3(HT)_1$. Samples made with $(HE)_2M_1T_1$, M_3T_1, and $(HE)_2M_1C_1^*$ all have similar permanent set, lower than the samples made with $M_2(HT)_2$ and $M_3(HT)_1$. On the other hand, stress whitening is highest for the samples made with $(HE)_2M_1T_1$, followed by the samples made with M_3T_1 and $(HE)_2M_1C_1^*$. The samples with $M_3(HT)_1$ show somewhat

less stress whitening, while those made with $M_2(HT)_2$ have the lowest stress whitening. A more detailed study would be needed to sort out all the operative mechanisms behind these observations, but this is beyond the scope of this work.

Figs. 11 and 12 show the Young's modulus and stress at 300% strain, respectively, of the nanocomposites prepared in this study. The addition of clay produces an increase in the Young's modulus of all the nanocomposites, even at low loadings. As the clay concentration increases, the nanocomposites made from $(HE)_2M_1T_1$ produce the largest increase in Young's modulus, while the ones made from $M_2(HT)_2$ present the smallest. Fig. 11a shows that the one-tailed organoclay leads to higher stiffness values than the two-tailed organoclay, while there is not much difference in the Young's modulus for nanocomposites based on the saturated and unsaturated organoclays. There is a significantly higher increase in Young's modulus of samples made from the organoclay containing $(HE)_2M_1T_1$ (Fig. 11b), suggesting that the hydroxy ethyl functional groups and a longer alkyl tail lead to greater TPU matrix reinforcement.

Fig. 12 shows that the stress at 300% elongation is highest in samples made from $(HE)_2M_1T_1$, while $M_2(HT)_2$ produces the lowest 300% stress overall. M_3T_1 and $(HE)_2M_1C_1^*$ produce a substantial increase in the 300% stress, even at high clay

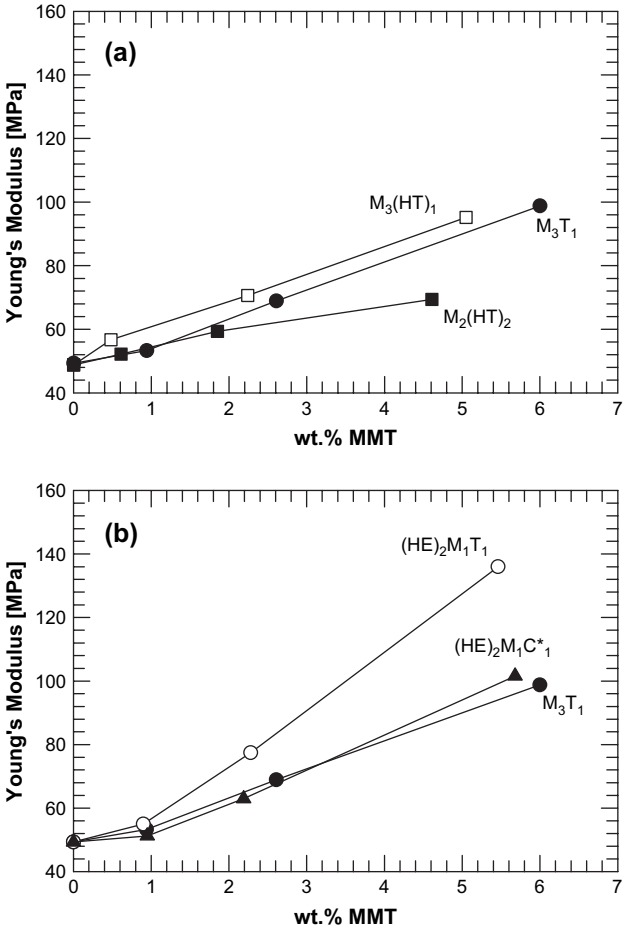

Fig. 11. Young's modulus of M-H TPU nanocomposites. (a) $M_3(HT)_1$, $M_2(HT)_2$, and M_3T_1 and (b) M_3T_1, $(HE)_2M_1T_1$, and $(HE)_2M_1C_1^*$.

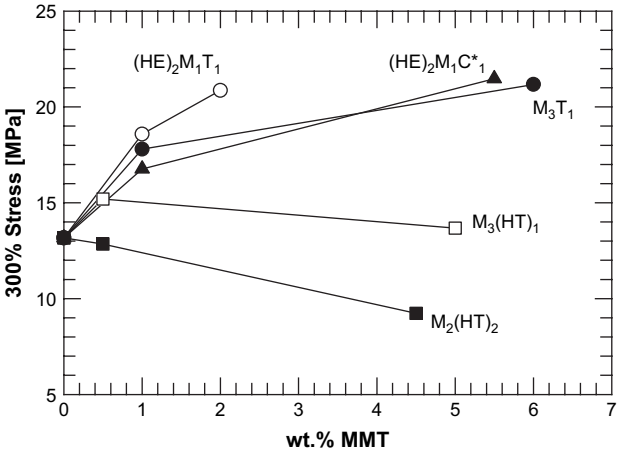

Fig. 12. 300% stress for M-H TPU nanocomposites.

concentration, as opposed to the behavior observed for $M_2(HT)_2$, where it gradually decreases with MMT concentration. On the other hand, the 300% stress for the samples made with $M_3(HT)_1$ increases slightly at low loadings and then remains almost constant. It should be noted that the 300% stress for the nanocomposites containing $(HE)_2M_1T_1$ is presented only at low concentrations, since the elongation at break is less than 300% for composites with higher concentrations.

The effect of organoclay structure on elongation at break could not be fully evaluated in this study since most of the samples prepared did not break before the Instron machine limit of 400% elongation. The only sample that broke before the 400% limit was the highest concentration sample made from $(HE)_2M_1T_1$. Reports in the literature show somewhat mixed results regarding the elongation at break. Some reports show an increase in elongation at break with increasing clay concentration and dispersion [2], some show a decrease [20–22], while others show a maximum of ultimate tensile properties at a low clay concentration (some mention 1 wt% and others mention 3 wt% of clay) [14–17,19,21,24,25].

The evidence described above suggests that the organoclay containing one long alkyl tail leads to better dispersion of MMT platelets and greater matrix reinforcement than the organoclay that contains two long alkyl tails. It was also seen that the unsaturated organoclay produces a very similar structure to that obtained from the saturated organoclay, which suggests that hydrogenating the tallow tail has no significant effects on morphology and mechanical properties. This was also found for PA-6, where Fornes et al. proposed that polar polymers like polyamides, and apparently polyurethanes, have a relatively good affinity for the polar clay surface and that the single tail represents the best balance between reducing the platelet–platelet attraction and allowing the polymer to have access to the silicate surface; two alkyl tails limit the access of the polymer chains to the clay surface to a greater extent [10]. It was also suggested that the saturated and unsaturated organic treatments may give very similar morphologies and degrees of reinforcement because they provide almost the same access of the polymer matrix to the clay surface. Evidently, the TPU matrix interacts favorably with the silicate

surface but not as well as PA-6, since the latter gives much higher platelet exfoliation. On the other hand, the results presented here also show that the organoclay with hydroxy ethyl functional groups leads to significantly higher clay dispersion and platelet exfoliation, producing a greater stiffness than the corresponding organoclay without these functional groups. This result deviates from what was seen for PA-6, where organoclays having methyl functional groups produce a much higher reinforcement. Fornes et al. suggested that the hydroxy ethyl groups provide some degree of shielding of the clay surface, where the −OH moiety may be attracted towards the polar clay surface [10]. Similar observations were reported for non-polar polymers, where organoclays that provide a higher shielding of the clay surface, i.e., $M_2(HT)_2$ and $(HE)_2M_1T_1$, gave better clay dispersion and matrix reinforcement [12]. Recently, Choi et al. showed that nanocomposites made from hydroxylated polyisoprene-*block*-polystyrene-*block*-polybutadiene (ISBOH) triblock copolymers had a higher degree of clay dispersion with $(HE)_2M_1T_1$ organoclay than those made from $M_2(HT)_2$-125. It was proposed that the presence of attractive interactions between the hydroxyl group of the ISBOH triblock copolymer and the hydroxyl group in the organoclay aided clay dispersion [34]. It seems like the hydroxy ethyl functional groups in the organoclay have the possibility to form hydrogen bonds with either the surface of the clay or the polar groups in the polymer matrix. In the case of TPU nanocomposites, we propose that the high affinity of the polymer matrix to the hydroxy ethyl groups in the organoclay might make hydrogen bonding with the polymer matrix more favorable, aiding clay dispersion and exfoliation. Reports in the literature have shown in general, that organoclays containing hydroxy ethyl functional groups lead to higher silicate dispersion and delamination in polyurethanes [16,18,20,21,24,25]. It is suggested that the hydroxy ethyl groups may match the polarity of the polyurethane matrix better than just having hydrocarbon chains, making dispersion more favorable [18].

3.1.3. Color formation

Fornes et al. and Yoon et al. [35,36] have described color formation for PA-6 and polycarbonate (PC) nanocomposites made with different organoclays. They showed that the level of color intensifies with clay content and that color formation depends on the nature of the organoclay used. Their study also indicates that organoclays with unsaturated surfactants lead to more color depth than organoclays with saturated structures, and that a deeper color was observed for the surfactant containing both hydroxy ethyl and unsaturated tallow. This is also true for these TPU nanocomposites. Fig. 13 shows how the color of M-H TPU nanocomposites varies with organoclay structure. This figure shows that all the samples have high optical transparency, as observed by Chang and An [17], and that organoclays containing a hydrogenated-tallow surfactant produce samples with a yellow tint, hydroxy ethyl functional groups produce a brown tone, while the unsaturated tallow surfactant generates a green hue. Fornes et al. and Yoon et al. mention that color formation is a product of clay-induced

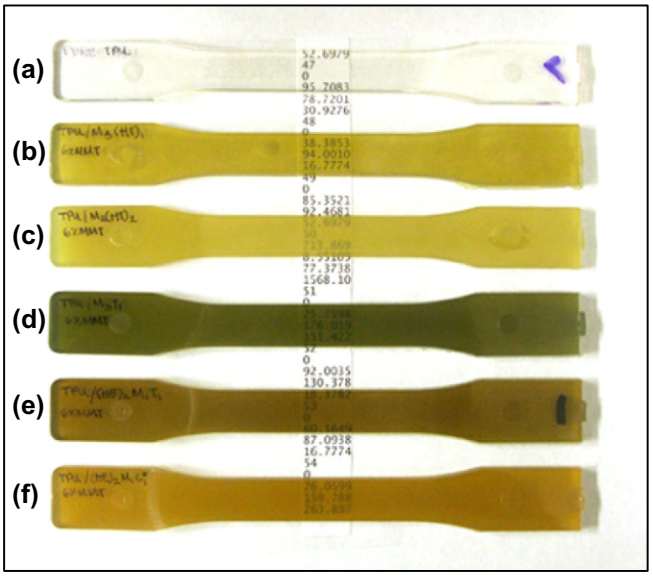

Fig. 13. Color formation of M-H TPU nanocomposites. (a) pure M- H TPU, (b)–(f) M-H TPU nanocomposites with ~5.5 wt% MMT: $M_3(HT)_1$, $M_2(HT)_2$, M_3T_1, $(HE)_2M_1T_1$, and $(HE)_2M_1C_1^*$ organoclays, respectively. (For interpretation of the references to color in this figure legend, the reader is referred to the web version of this article.)

chemical reactions, such as matrix degradation and/or surfactant stability, and that a higher dispersion leads to a greater exposure of the clay surface and, hence, a greater opportunity for chemical reaction [35,36]. PA-6 and PC nanocomposites only show shades of yellow and brown, while some TPU nanocomposites show shades of green as well. A clay purification experiment was done to determine if the greenish hue was produced by clay impurities. M_3T_1 organoclay was purified with methanol, and was later used to make TPU nanocomposites. The same green tint was observed in these samples, so we conclude that the green color formation is not due to clay impurities. Taking this into account, we suggest that the different colors may arise from specific chemical interactions between the specific organic treatment and the polymer material or additives therein.

3.2. Structure and properties for the H-H TPU

Thermoplastic polyurethanes are composed of hard and soft segments, formed by aromatic isocyanates and long-chain diols. These segments segregate, like in semi-crystalline polymers, having a direct effect on the properties of the material. The long-chain diols are mainly polyether- or polyester-based, and the type of long-chain diol used also affects the properties of the final TPU. Reports in the literature suggest that the structure of TPU materials, such as type of polyol and ratio of soft to hard segments, affects the mechanical properties and morphology of their nanocomposites [16,20].

A series of nanocomposites were made from the high-hardness TPU described earlier and $(HE)_2M_1T_1$ and $M_3(HT)_1$ organoclays. The results are compared to the nanocomposites made from the medium-hardness TPU described in the previous section in an effort to explore the effect of different types of TPU

materials on morphology and properties of nanocomposites. The high-hardness TPU is a polyether-based TPU with a Shore D hardness of 73 D, while the medium-hardness TPU is a polyester-based TPU with a Shore D hardness of 58 D. The monomer precursors for the high-hardness TPU are MDI and polytetrahydrofuran, while the medium-hardness TPU is made from MDI, 1,4-butanediol, and ε-caprolactone. The differences in these TPU's were evidenced, in part, during the injection molding of these materials and its nanocomposites. The high-hardness materials required lower barrel temperatures, shorter injection times, longer cooling times, and a lower mold temperature for injection molding. For this TPU, no TEM images or mechanical testing are shown at high MMT concentrations since such samples could not be produced because the current injection molding machine could not achieve the low molding temperatures needed.

3.2.1. Clay dispersion

WAXD patterns in Fig. 14 show basal reflections for the H-H TPU nanocomposites, indicating the presence of tactoids. The *d*-spacing for the medium-hardness TPU, as mentioned before, increases from 1.77 to 3.05 nm and from 1.8 to 2.9 nm for hydroxy ethyl and one-tailed organoclays, respectively; while the H-H TPU nanocomposites show a low broad peak at 3.25 nm and an intense peak at 3.22 nm for $(HE)_2M_1T_1$ and $M_3(HT)_1$ organoclays, respectively.

Fig. 15 compares high magnification TEM images of these nanocomposites based on the two types of TPU. In both cases, the number of particles is higher for the samples made with hydroxy ethyl organoclay, where the particles are smaller in size and a larger number of single platelets exist. Even though the MMT concentration of the TEM micrograph for the M-H TPU/$M_3(HT)_1$ sample is lower than the MMT concentration of the other micrographs, particle analysis results shown previously show that the specific particle density of M-H TPU/$M_3(HT)_1$ nanocomposites at 1 wt% MMT is significantly lower than those made with $(HE)_2M_1T_1$, which is in accord with our observations.

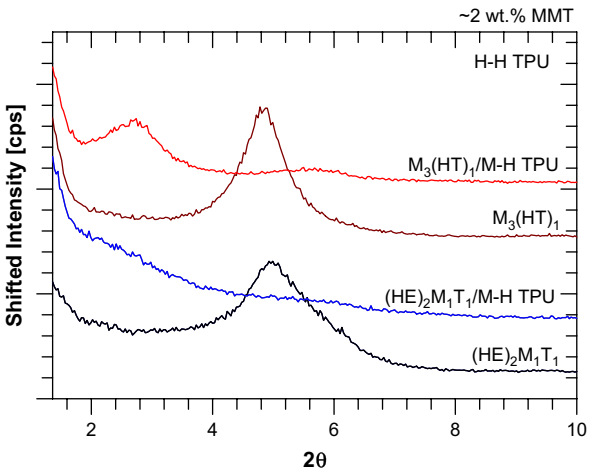

Fig. 14. WAXD patterns of $M_3(HT)_1$ and $(HE)_2M_1T_1$ organoclays and its high-hardness TPU nanocomposites.

3.2.2. Mechanical properties

The stress–strain behavior of the M-H and H-H TPU nanocomposites with $(HE)_2M_1T_1$ organoclay is compared in Fig. 16. The stress–strain diagrams of the pure H-H TPU and its nanocomposites have a very different shape than those from M-H TPU; a yield point is observed for the H-H TPU materials, while no distinct yield point is observed for the M-H TPU nanocomposites. Regardless of clay concentration, the stress levels for the H-H TPU samples are much higher than that of the M-H TPU samples. H-H TPU samples, unlike the M-H TPU samples, show a yield point, after which a distinct drop in tensile stress is observed indicating the onset of necking. As the clay concentration increases the stress increases, similar to the behavior observed for the M-H TPU nanocomposites.

Fig. 17 shows the Young's modulus of the nanocomposites made from H-H TPU at different MMT concentrations. The moduli of the H-H TPU matrix and its composites are much higher than the corresponding M-H TPU matrix and composites. Nevertheless, both TPU's have the same response to organoclay structure, i.e., better reinforcement is obtained with the hydroxy ethyl organoclay. The medium-hardness TPU shows a large increase in modulus with increasing wt% MMT, while in the high-hardness samples, $(HE)_2M_1T_1$ shows almost no enhancement until 1 wt% MMT and almost no enhancement at all for the one-tailed organoclay. This difference in modulus enhancement may be due in part to the considerably lower modulus of the M-H TPU matrix. As stated by Fornes et al. low-modulus matrices offer a higher potential for reinforcement than high-modulus matrices, for a given filler aspect ratio, as a result of the larger ratio of filler to matrix moduli. As this ratio increases, the nanocomposite modulus becomes more sensitive to the aspect ratio of the filler, so a larger increase in modulus may not suggest a higher degree of exfoliation or reinforcement [37]. This was also mentioned by Finnigan et al. for TPU nanocomposites [20].

The elongation at break also shows significant differences between the two types of TPU's. H-H TPU nanocomposite samples show noticeable necking, and the elongation at break was lower than the 400% machine limit (Fig. 18). The elongation at break in the samples made with the H-H TPU matrix remains almost constant for the one-tailed organoclay while it decreases significantly with the hydroxy ethyl organoclay. This is consistent with the levels of reinforcement obtained with these two organoclays. Since the elongation at break of the M-H TPU could not be fully explored due to machine limitations, we cannot give any conclusions regarding the effect of the different types of TPU's on elongation at break. Tien and Wei show an increase in Young's modulus and a decrease in elongation at break with increasing hard segment concentration [16]; the results here show an indication of similar behavior.

Overall, both types of TPU's show the same trends with respect to organoclay structure, e.g., better clay dispersion and enhancement of mechanical properties are observed for the organoclay containing hydroxy ethyl functional groups as compared to the organoclay with one-tailed hydrogenated-tallow

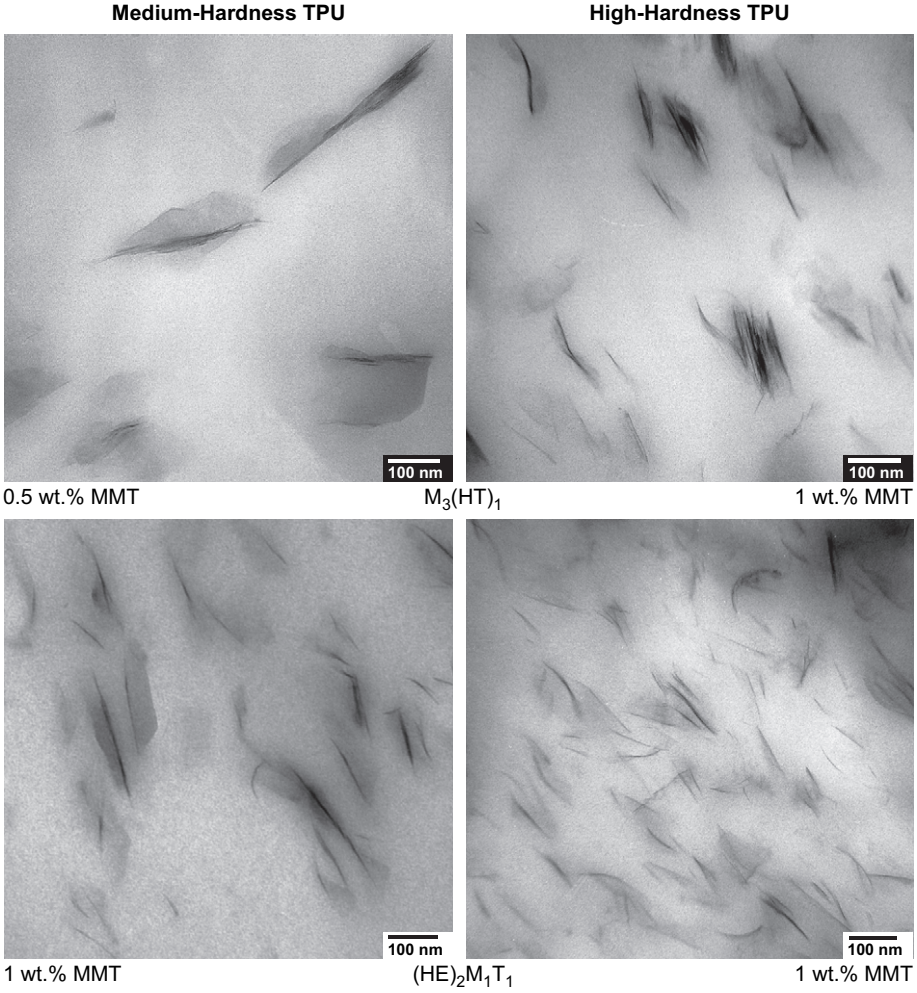

Fig. 15. TEM micrographs of medium-hardness and high-hardness TPU nanocomposites containing $(HE)_2M_1T_1$ and $M_3(HT)_1$ organoclays.

substituents. This supports the reasoning made in the previous section where it was proposed that the hydroxy ethyl functional groups lead to higher degrees of clay dispersion of TPU nanocomposites. Apparently, the soft to hard segment ratio and/or polyol structure have a noticeable effect on the morphology and mechanical properties of TPU nanocomposites. H-H TPU nanocomposites showed a slightly higher number of particles and clay dispersion, i.e., better exfoliation. However, adding clay to the M-H TPU causes a greater improvement in relative modulus, e.g., at a concentration of

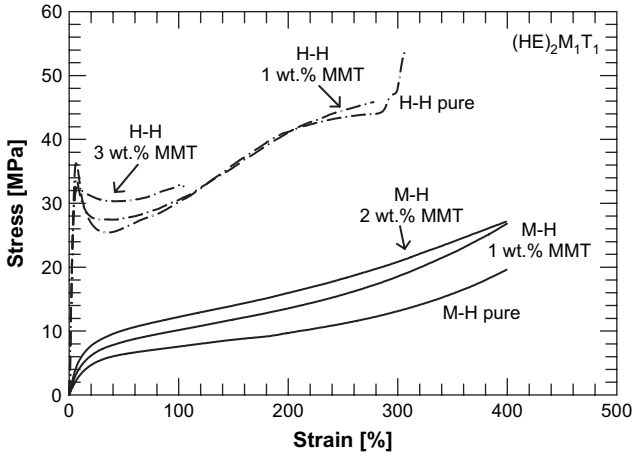

Fig. 16. Stress–strain curves for medium-hardness and high-hardness TPU's and its nanocomposites containing $(HE)_2M_1T_1$ organoclay.

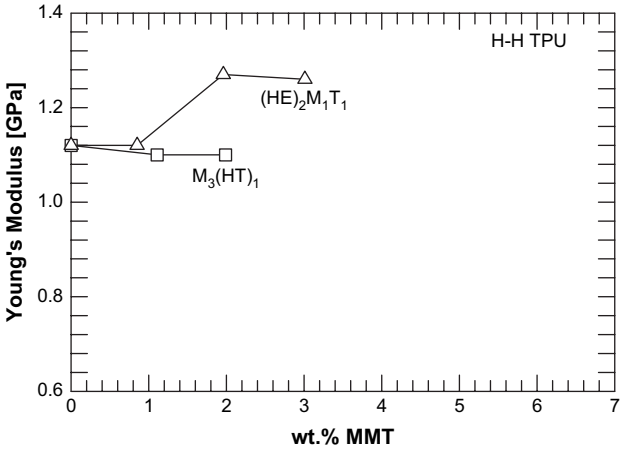

Fig. 17. Young's modulus of high-hardness TPU nanocomposites containing $(HE)_2M_1T_1$ and $M_3(HT)_1$ organoclays.

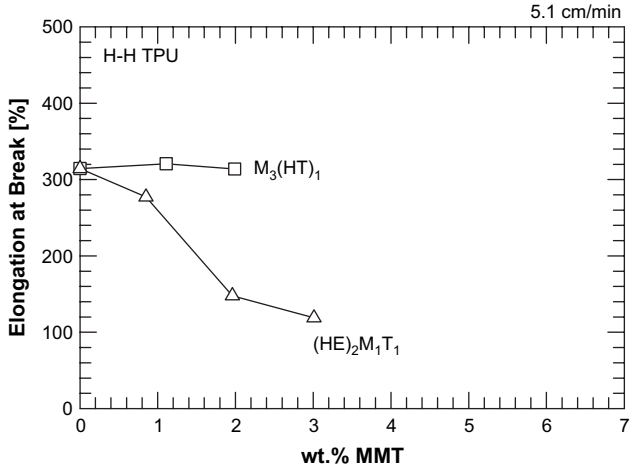

Fig. 18. Elongation at break of high-hardness TPU nanocomposites containing $(HE)_2M_1T_1$ and $M_3(HT)_1$ organoclays.

~2 wt% MMT, the relative modulus for $(HE)_2M_1T_1$ nanocomposites made from the M-H TPU is 1.57, while it is 1.13 for the nanocomposites made from the H-H TPU. The primary reason for the greater relative modulus in the case of M-H TPU nanocomposites is due to the much lower absolute modulus of the M-H matrix, as predicted by composite theory [37].

Self-consistent field theory calculations suggest that the polar hard segments are attracted towards the silicate surface while the non-polar soft segments separate the individual platelets to regain entropy [38]. The structure of the TPU has an effect on the polarity of the polymer molecules, and different levels of polarity influence the affinity between the polymer and the organoclay. It is proposed here that these two materials interact differently with the organoclay, and the structure of the TPU may lead to differences in clay dispersion and relative mechanical property enhancement; however, at this point, it is not possible to be more definitive about the underlying causes for this difference.

4. Conclusion

Structure–property relationships for TPU nanocomposites prepared by melt processing from a series of alkyl ammonium/MMT organoclays and medium-hardness and high-hardness thermoplastic polyurethanes are presented here. The structure of the organic modifier used to form the organoclay was systematically varied to determine the effect of specific functional groups on the degree of clay dispersion and matrix reinforcement for M-H TPU nanocomposites. Morphology analysis and mechanical property results show that overall, the $(HE)_2M_1T_1$ surfactant produces the best dispersion of organoclay particles and the highest matrix reinforcement, while the $M_2(HT)_2$ surfactant produces the lowest. More specifically, the results show (a) one long alkyl tail on the ammonium ion rather than two, (b) hydroxy ethyl groups on the amine rather than methyl groups, and (c) a longer alkyl tail as opposed to a shorter one leads to higher clay dispersion and stiffness enhancement for TPU nanocomposites. Most of these trends are similar to what was observed in PA-6 based nanocomposites, which suggests that polar polymers like polyamides, and apparently polyurethanes, have a relatively good affinity for the polar clay surface; and in the case of polyurethanes, the high affinity of the matrix for the hydroxy ethyl functional groups in the $(HE)_2M_1T_1$ organoclay aids clay dispersion and exfoliation. This suggests that an organic treatment that provides the best balance between reducing platelet–platelet attraction and increasing organoclay–polymer affinity will produce a higher degree of clay dispersion. A more limited study comparing a medium-hardness polyester-based TPU and a high-hardness polyether-based TPU shows that both types of TPU's exhibit similar trends with respect to organoclay structure, supporting the previous reasoning. Apparently the soft to hard segment ratio and/or polyol structure have a noticeable effect on the morphology and mechanical properties of TPU nanocomposites. H-H TPU nanocomposites showed a slightly higher number of particles and clay dispersion, i.e., better exfoliation. However, because of the much lower modulus of the M-H TPU, adding clay to this matrix causes a greater improvement in relative modulus. Finally, it should be noted that even though some organoclays lead to TPU nanocomposites with high degrees of clay dispersion and platelet exfoliation, none exhibited degrees of exfoliation as high as those observed in PA-6 nanocomposites. Nevertheless, this study provides insights about the effect of the organoclay structure and polarity of the polymer matrix on morphology and mechanical properties of polymer–clay nanocomposites.

Acknowledgements

This work was funded by the Air Force Office of Scientific Research and by the Consejo Nacional de Ciencia y Tecnología (CONACyT) of Mexico. The authors would like to thank Southern Clay Products Inc. for providing the clay materials and WAXD analyses. We also acknowledge Dr. Desiderio Kovar and Dr. John Mendenhall for several helpful discussions.

References

[1] Liu L, Qi Z, Zhu X. J Appl Polym Sci 1999;71(7):1133–8.
[2] Wang Z, Pinnavaia TJ. Chem Mater 1998;10(12):3769–71.
[3] Hu Y, Wang S, Ling Z, Zhuang Y, Chen Z, Fan W. Macromol Mater Eng 2003;288:272–6.
[4] Schmidt D, Shah D, Giannelis EP. Curr Opin Solid State Mater Sci 2002;6(3):205–12.
[5] Yano K, Usuki A, Okada A, Kurauchi T, Kamigaito O. J Polym Sci Part A Polym Chem 1993;31(10):2493–8.
[6] Messersmith PB, Giannelis EP. J Polym Sci Part A Polym Chem 1995;33(7):1047–57.
[7] Chen W, Xu Q, Yuan RZ. Mater Sci Eng B Solid State Mater Adv Technol 2000;B77(1):15–8.
[8] Chen W, Xu Q, Yuan RZ. Compos Sci Technol 2001;61(7):935–9.
[9] Yoon PJ, Fornes TD, Paul DR. Polymer 2002;43(25):6727–41.
[10] Fornes TD, Yoon PJ, Hunter DL, Keskkula H, Paul DR. Polymer 2002;43(22):5915–33.
[11] Hotta S, Paul DR. Polymer 2004;45(22):7639–54.

[12] Shah RK, Hunter DL, Paul DR. Polymer 2005;46(8):2646–62.
[13] Lee HS, Fasulo PD, Rodgers WR, Paul DR. Polymer 2005;46(25): 11673–89.
[14] Chen TK, Tien YI, Wei KH. Polymer 2000;41(4):1345–53.
[15] Tien YI, Wei KH. Macromolecules 2001;34(26):9045–52.
[16] Tien YI, Wei KH. Polymer 2001;42(7):3213–21.
[17] Chang J-H, An YU. J Polym Sci Part B Polym Phys 2002;40(7):670–7.
[18] Osman MA, Mittal V, Morbidelli M, Suter UW. Macromolecules 2003; 36(26):9851–8.
[19] Choi WJ, Kim SH, Kim YJ, Kim SC. Polymer 2004;45(17):6045–57.
[20] Finnigan B, Martin D, Halley P, Truss R, Campbell K. Polymer 2004;45(7):2249–60.
[21] Finnigan B, Martin D, Halley P, Truss R, Campbell K. J Appl Polym Sci 2005;97(1):300–9.
[22] Xiong J, Liu Y, Yang X, Wang X. Polym Degrad Stab 2004;86(3): 549–55.
[23] Pattanayak A, Jana SC. Polymer 2005;46(14):5183–93.
[24] Pattanayak A, Jana SC. Polymer 2005;46(10):3394–406.
[25] Pattanayak A, Jana SC. Polymer 2005;46(10):3275–88.
[26] Song L, Hu Y, Li B, Wang S, Fan W, Chen Z. Int J Polym Anal Charact 2003;8(5):317–26.
[27] Karger-Kocsis J. ‘‘Nanoreinforcement’’ of thermoplastic elastomers. In: Fakirov S, editor. Handbook of condensation thermoplastic elastomers. Wiley-VCH; 2005. p. 473–88.
[28] Cho JW, Paul DR. Polymer 2000;42(3):1083–94.
[29] Fornes TD, Yoon PJ, Keskkula H, Paul DR. Polymer 2001;42(25): 9929–40.
[30] Vaia RA, Giannelis EP. Macromolecules 1997;30(25):7990–9.
[31] Layers are similar to transparent sheets stacked on top of the original image. Layers allow one to draw or trace elements of the image without modifying the original. One can see through a layer to the ones below in the regions that are blank.
[32] Chavarria F, Paul DR. Polymer 2004;45(25):8501–15.
[33] The ‘Image Processing Tool Kit’ allows one to measure particle lengths and areas of particles contained in subsequent layers, within Adobe Photoshop.
[34] Choi S, Lee KM, Han CD. Macromolecules 2004;37(20):7649–62.
[35] Fornes TD, Yoon PJ, Paul DR. Polymer 2003;44(24):7545–56.
[36] Yoon PJ, Hunter DL, Paul DR. Polymer 2003;44(18):5341–54.
[37] Fornes TD, Paul DR. Polymer 2003;44(17):4993–5013.
[38] Balazs AC, Singh C, Zhulina E. Macromolecules 1998;31(23):8370–81.